Low density interior in supercooled aqueous nanodroplets expels ions to the subsurface

Shahrazad M. A. Malek,[1] Ivan Saika-Voivod,[1] and Styliani Consta[2]

[1] *Department of Physics and Physical Oceanography, Memorial University of Newfoundland, Canada, A1B 3X7*

[2] *Department of Chemistry, The University of Western Ontario, London, Ontario, Canada N6A 5B7*

(Dated: March 19, 2021)

The location of a single and multiple ions in aqueous droplets plays a key role in chemical reactivity of atmospheric and man-made aerosols. We report direct computational evidence that in supercooled aqueous nanodroplets a lower density core of tetrahedrally coordinated water expels the sodium ions to a higher density and more disordered subsurface. In contrast, at ambient temperature the single Na^+ density is higher in the core region and has a broad maximum at the droplet's center of mass. We analyse the expulsion of a single ion in terms of a general reference electrostatic model that we have developed. The energy of the system in the analytical model is expressed as the sum of electrostatic and surface energy of a fluctuating droplet. The model predicts that the energy associated with the distance of the ion from the droplet's center of mass is quadratic in this distance. We name this effect "electrostatic confinement". The predictions of the model are consistent with the simulations' findings for a single Na^+ ion at ambient conditions. Our results assist in understanding the mechanisms of charging of macromolecules in spray-based ionization methods used in native mass spectrometry and the physical chemistry of atmospheric aerosols.

I. INTRODUCTION

The location of ions in droplets plays a key role in determining reactivity in atmospheric and man-made aerosols. Applications of the man-made aerosols relevant to this study include ionization methods of bulk solution intended for mass spectrometry analysis and use of droplets as micro- (nano-) reactors for accelerating chemical synthesis[1–3]. Aerosol droplets in the lower atmosphere carry a small charge determined by at most a few excess ions whereas droplets in thunderclouds and electrosprays are highly charged. The location of ions in droplets may be affected by temperature because the temperature determines the physical state of the solvent. In this article we study the structure of supercooled aqueous mesoscopic clusters charged with a single and multiple ions. Hereafter, we will use the term nanodroplet for a mesoscopic clusters.

Numerous computational studies [4–23] and experiments[22, 24–28], have examined the location of a single akali and halogen ion in clusters comprised up to a few tens of water molecules. The most of the research is for clusters at ambient conditions. The supercooled clusters have been simulated less because they are notoriously challenging to equilibrate.

Voth and co-workers[11] have studied the location of a single Na^+, Cl^- and H_3O^+ ion in clusters of $H^+(H_2O)_{100}$, $Na^+(H_2O)_{20}$, $Na^+(H_2O)_{17}$, $Na^+(H_2O)_{100}$ and $Cl{-}(H_2O)_{17}$ in the temperature range of 100 K-450 K. They found that below the freezing temperature in clusters of 100 H_2O molecules H_3O^+ and Na^+ were excluded from the cluster interior and tend to reside within a few monolayers of the surface. Above the cluster melting point, both the Na^+ and Cl^- ion tend to be found closer to the center. In supercooled clusters of 20 H_2O molecules the Na^+ ion is found in the center. The central location is attributed to the fact that in such a small cluster where all the H_2O molecules are on the surface, thus, there is no other location for the Na^+ ion than the interior, since its exposure in the air is not energetically favourable. The Cl^- ion in a cluster of 17 H_2O molecules is distinctly found on the cluster surface.

Zhao et al.[9] performed simulations of halogen anions in a cluster of 124 H_2O molecules using Born-Oppenheimer molecular dynamics simulations. It was found that Br^- and I^- tend to be located near the surface region of a supercooled water droplet, whereas F^- exhibits interior solvation. The Cl^- ion exhibits no strong tendency for surface or interior solvation at a supercooled condition and at room temperature.

The studies of the location of multiple ions in nanodroplets are a few. Previously[29–31] we have reported atomistic simulations of the location of multiple ions in aqueous nanodroplets with diameter $\approx$ 2 nm - 16 nm at a temperature range of 300 K to 450 K. We have found that in droplets comprised $\approx$ 1000 H_2O molecules the radial ion distribution (measured from the droplet's center of mass) is almost uniform. As the droplet size increases, the distribution shows a distinct maximum in the outer droplet layers. The distribution dies off toward the droplet's COM by a slow almost exponential decay. Towards the droplet exterior, the decay is determined by a characteristic length arising from the solution of the Non-linear Poisson-Boltzmann equation (NPB), the ion size and shape fluctuations[29]. The solution of NPB equation for a spherical geometry was used as a reference model to compare with the atomistic simulations. The distribution of the multiple ions at supercooling is still completely unknown.

Here we study the location of a single ion in relation to the water structure in supercooled droplets with sizes that vary from 100 H_2O molecules (corresponding di-

N (H_2O)	L (nm)	T (K)	$N_{\rm Na}$	$t_{\rm run}$ (μs)	$N_{\rm d}$	R_e (nm)	τ (ns)
100	10	200	1	1.6	100	0.87	0.4
		260	1	1.6	99.8		0.8
200	10	200	1	1.6	200	1.10	0.8
		260	1	1.6	199.8		0.8
360	10	200	1	1.6	360	1.35	0.4
		200*	1	0.44	360	1.35	0.4
		300	1	1.6	359.3	1.35	0.2
776	15	200	1	0.33	776	1.77	0.8
		200*	1	0.46	776	1.77	0.8
		200*	5	0.53	776	1.77	0.8
		300	1	0.77	773.9	1.75	0.4
1100	20	200	1	0.32	1100	2.0	1.6
		200*	8	0.055	1100	2.0	1.6
		300	1	0.32	1095.1	1.97	0.8

TABLE I. Simulation parameters. N denotes the number of H_2O molecules in the simulation box of dimension L. N_d is the average number of the H_2O molecules that form a connected drop, τ is the relaxation time and $t_{\rm run}$ is the duration of the run. The "*" superscript in the temperature refers to simulations started with Na^+ ion(s) in the droplet center. R_e denotes the equimolecular radius.

ameter $\approx$ 1.8 nm) to 1100 (corresponding diameter $\approx$ 4.0 nm). In addition we present the first study of the location of multiple ions in supercooled droplets. We find that at supercooling, in droplets larger than 100 H_2O molecules, a low density core of randomly oriented tetrahedra forms that expels the ions to the higher density and more disordered outer droplet layers. The distinct water structure of supercooled nanodroplets[32] (without the presence of ions) has also been observed in simulations of nucleation within droplets and thin films [33–36]. The increased concentration of the ions in the outer layer will affect the reactivity in atmospheric aerosols and charge transfer reactions that macromolecules undergo in spray-based ionization methods used in native mass spectrometry. Despite the numerous studies of a single ion in clusters, a reference model of a single ion solvation in a droplet is still missing from the literature. In this study we provide a continuum model that considers a fluctuating charged dielectric droplet. The energy in the model is written as the sum of the electrostatic energy and the surface energy. The model finds that the energy associated with the distance of the ion from the droplet COM is quadratic in this distance. We name this effect "electrostatic confinement".

II. MODELS AND SIMULATION METHODS

We simulate Na^+ ions in aqueous nanodroplets at T =200 K, 260 K, and 300 K, representing ambient and supercooled conditions. The system sizes and length of simulations are shown in Table 1. The simulations are performed by molecular dynamics (MD) as implemented in Gromacs v4.6.1 [37–40]. The water molecules are modeled with the TIP4P/2005 (transferable intermolecular potential with four points) model [41]. For Na^+ the OPLS-AA parameters are taken from Ref. [42]. Specifically, the ion has charge +1.00 e (where e is the elementary positive charge), and Lennard-Jones parameters ϵ = 0.0115980 kJ/mol, and σ =0.333045 nm. In interacting with the O site of the water molecules the combining rules $\epsilon_{Na,O} = \sqrt{\epsilon_{Na}\epsilon_O}$ and $\sigma_{Na,O} = \sqrt{\sigma_{Na}\sigma_O}$ are used.

Each nanodroplet has been placed in a periodic cubic box of length L (see Table 1). The box is large enough to avoid any interaction between the water droplet and its periodic images. The length of cutoff for interactions (Coulomb and Lennard-Jones) is at $L/2$, which is much larger than the droplet's diameter so as it includes the shape fluctuations. The simulations are carried out in the canonical ensemble – constant number of molecules N, volume V, and T. The temperature is controlled by using the Nosé-Hoover thermostat with time constant 0.1 ps. The equations of motion are integrated with the leap-frog algorithm with a time step of 2 fs.

The simulations are initiated with a condensed pure water nanodroplet where the Na^+ ions are placed at the surface for the majority of the single Na^+ runs, and in the center for two runs at $N = 360$ and 776 at $T = 200$ K. All runs with multiple Na^+ ions start with the ions near the droplet center of mass.

In Table I, the mean number of molecule, N_d, participating in the liquid droplet (those not in the vapor), and the relaxation time τ, determined from the neighbour correlation function are shown[32]. The values of τ provide an estimate for the relaxation time for simulations that include ions. In the temperature range where simulations are performed the solvent evaporation within the simulation box is negligible.

To ensure that the we sufficiently sample an equilibrated system after the addition of a single Na^+ ion at 200 K, where the concern for equilibration is the highest, we run two simulations for each of $N = 360$ and $N = 776$ nanodroplets. In one set, we set the Na^+ ion at or near the centre of the droplet, quench the system through a conjugate-gradient energy minimization, and then proceed with MD simulation. In the other, we initially place the ion on the surface. Equilibration is achieved when results converge from the two simulations. For example, for $N = 776$ after 400 ns, the ion densities as a function of radial distance from the centre of mass of the droplet $\rho_{\rm ion}(r)$ converge for the two simulations. For $N = 1100$, we assume that the equilibration time is longer by a factor of $\tau_{1100}/\tau_{776} \approx 2$. For multiple ions, initially distributed in the nanodroplet interior, we expect to be approximately the same as the single ion simulations.

To help understand the features of $\rho_{\rm ion}(r)$ in terms of the structure of pure water nanodroplets, we report a few other quantities as a function of radial distance from the pure water nanodroplet centre of mass (COM). These include the density of water $\rho(r)$, the density of water as determined from the Voronoi volumes associated with

each water molecule $\rho_v(r)$, the tetrahedral order parameter $q_T(r)$ and the distance to the fifth nearest neighbour O of a given O atom d_5.

In our previous study [32], the Voronoi cells for all O sites were computed, while the H sites were ignored. Within each shell of radius r, the total volume $\mathcal{V}(r)$ of the Voronoi cells for O sites was found, and the same for the number of O sites in the shell, $\mathcal{N}(r)$. The average density as determined by the Voronoi cell volumes is defined as $\rho_{\rm v}(r) = m\langle \mathcal{N}(r)/\mathcal{V}(r)\rangle$, where $\langle \cdots \rangle$ indicates an average over the configurations sampled in the simulations, and m is the mass of a water molecule.

To characterize the local structures, we determine the tetrahedral order parameter, which is defined at the level of a single particle as [43],

$$q_i = 1 - \frac{3}{8}\sum_{j=1}^{3}\sum_{k=j+1}^{4}\left[\cos\psi_{jik} + \frac{1}{3}\right]^2 \qquad (1)$$

where ψ_{jik} is the angle between an oxygen atom i and its nearest neighbour oxygen atoms j and k within a distance of $r_{cut} = 0.35$ nm. However, if there are more than four neighbour oxygen atoms within r_{cut}, we only consider the first four nearest neighbour oxygen atoms. We define the radial function $q_T(r)$ as the average value of q_i for all molecules within a spherical shell enclosed within $r \pm \Delta r/2$, where $\Delta r = 0.05$ nm. Similarly, we report results for $d_5(r)$, the average distance to the fifth O neighbour for O atoms located in the same spherical shell centered at r. Data for both $q_T(r)$ and $d_5(r)$ are taken from Refs. [44].

III. RESULTS

A. Single Na^+ ion

In Fig. 1, we plot $\rho(r)$ and $\rho_v(r)$ for pure water nanodroplets of all sizes studied at high (300 K for $N \geq 200$, 260 K for $N \leq 200$) and low (200 K) temperature (T), with data taken from Ref. [32]. At high T, shown in Fig. 1a, $\rho(r)$ is that of a typical liquid droplet, characterized by a flat (slowly decreasing) curve in the interior that decays sigmoidally to (near) zero over approximately an intermolecular distance at the liquid-vapor interface. The exceptions are the curves for $N \leq 200$ K, that at 260 K show some ordering or layering particularly near the surface. At low T, shown in Fig. 1b, there is significant layering for all nanodroplet sizes, and, as seen particularly well for the larger nanodroplets, an increase in density as r increases towards the surface. Note that for $r < 0.2$ nm, good statistics are difficult to obtain for all radial quantities, and results in this regime are quite noisy.

The undulations in $\rho(r)$ associated with layering make it difficult to characterize how the local density changes with r, and for this reason we plot $\rho_v(r)$. Fig. 1c shows $\rho_v(r)$ monotonically decreasing (or flat) with r for all nanodroplet sizes at high T. $\rho_v(r)$ is significantly smoother than $\rho(r)$, as it does not depend on the number density itself, but rather on the Voronoi volume surrounding each water molecule. An important feature of $\rho_v(r)$ is that it begins to decay to zero approximately 0.3 nm, or an intermolecular distance, before $\rho(r)$; Voronoi volumes are very large, and Voronoi-based density very low, for molecules on the surface. Molecules falling within the range where $\rho_v(r)$ is high (near bulk values) are completely surrounded by other water molecules and are not on the surface. Surface molecules can be identified as those located where $\rho_v(r)$ is small, and molecules in the subsurface as those located an intermolecular distance below the point at which $\rho_v(r)$ has decayed to near zero.

Fig. 1d shows $\rho_v(r)$ for nanodroplets at low T. For $N \geq 200$, there is a signifcant increase in density in the subsurface layer. The density may well be higher for surface molecules, but $\rho_v(r)$ can not characterize this. This increased density at low T appears to be a hallmark of cold water nanodroplets, and has not been reported for simple liquids to our knowledge. It is this heterogeneous environment in pure water that lends an interesting backdrop for studying ion distributions at low T.

In Fig. 1e, we plot $\rho_{Na}(r)$ at high T for systems composed of a single Na^+ ion within a nanodroplet. Since the ion density is quite high for small nanodroplets, we divide $\rho_{Na}(r)$ by 10 and 3 for $N = 100$ and 200, respectively. In all cases, the $\rho_{Na}(r)$ is approximately constant in the interior of the droplet, and begins to decay within the subsurface, and has decayed to zero significantly before $\rho(r)$ does. For a pure dielectric sphere at $T = 0$, a point charge has lowest energy at the centre of a sphere. At finite T, there will be a finite width associated with the distribution of ion position. In Appendix A, we present a theory for a single ion in a dielectric droplet that predicts a Gaussian $\rho_{Na}(r)$ (centred at $r = 0$), and our results are at least in qualitative agreement with this prediction.

Fig. 1f shows a dramatic difference in $\rho_{Na}(r)$ at low T. Rather than being centred at $r = 0$, the peak of $\rho_{Na}(r)$ is located within 0.1 nm of the peak in $\rho_v(r)$ (for $N \geq 200$). Thus, we see that in a nanodroplet with a heterogeneous radial density, as determined by $\rho_v(r)$, the single Na^+ ion tends to reside in the highest density environment. This tendency is consistent with the fact that for constant T and polarization factor (degree of dipole ordering) [45], the dielectric constant increases with increasing density. While the surface layer is at very high density, as measured by $\rho(r)$, clearly the surface does not provide a good solvation environment.

For $N = 100$ at low T, $\rho_v(r)$ is approximately constant for $r < 0.3$ nm, and then decreases with increasing r. While a constant $\rho_v(r)$ for $r < 0.3$ nm suggests that $\rho_{Na}(r)$ should be uniform in this interior region, we see that $\rho_{Na}(r)$ is in fact peaked just below 0.3 nm. We do see, however, that the peak in $\rho_{Na}(r)$ coincides with a local minimum in $\rho(r)$, suggesting that layering may play a significant role in determining where the Na ion

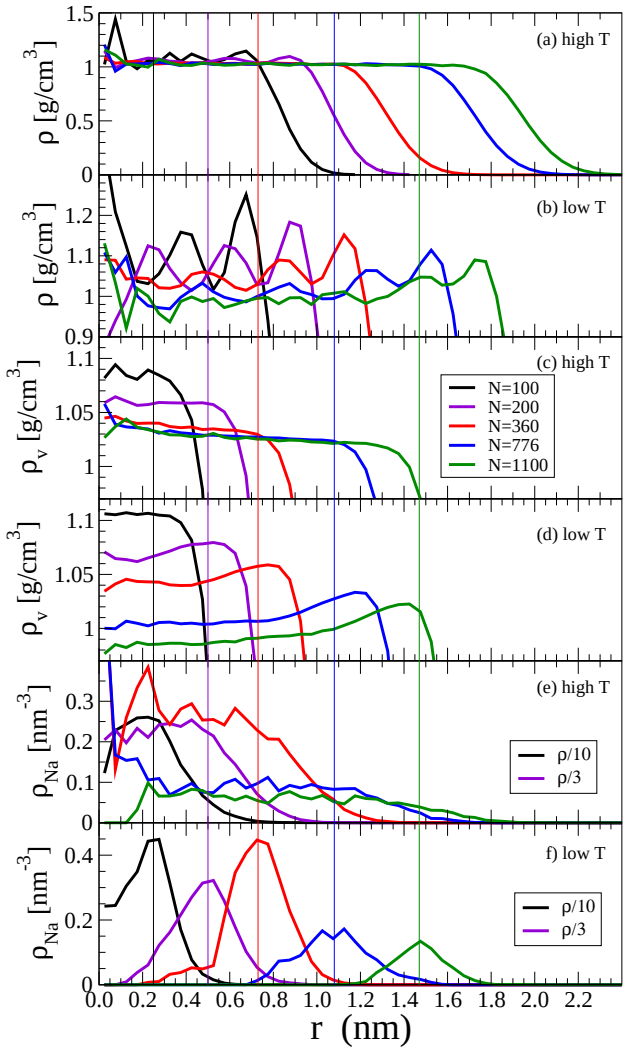

FIG. 1. Pure water nanodroplet structure and single Na^+ number density distributions for low temperature (T = 200 K) and high temperatures (T = 260 K for $N \leq 200$ and T = 300 K for $N \geq 360$). Panels (a) and (b) show water density $rho(r)$; panels (c) and (d) show water density based on molecular Voronoi volumes $\rho_v(r)$. Panels (e) and (f) show Na^+ number density $\rho_{\rm Na}(r)$, which for N = 100 and N = 200 have been reduced by a factor of 10 and 3, respectively. Note: to convert from molecule/nm^3 to mol/L, multiply by 10/6.022.

resides.

To probe the relationship between ion location and density a little further, we focus on the behaviour of the N = 776 nanodroplet at T = 200 K and T = 300 K in Fig. 2: In panel (a) we replot $\rho(r)$ and $\rho_v(r)$ for pure water, showing their full range of values, confirming that the surface layer is approximately 0.3 nm thick; in panel (b) we show a close-up of $\rho_v(r)$ that contrasts the monotonic decrease at high T with the monotonic increase towards a subsurface peak; in panel (c) we compare at low T $\rho_{Na}(r)$ as obtained from starting the ion near the centre and starting near the surface – thus showing the degree of equilibration we achieve; panel (d) shows that the ion density when five Na^+ ions are present in the nanodroplet shift at low T to have a peak at approximately the same r as for the single ion case; panel (e) shows the radial dependence of the tetrahedrality parameter, which has anapproximately constant value at high T, while at low T shows a significant decrease coinciding with the subsurface density peak; and panel (f) shows the radial dependence of d_5, a more indirect measure of the quality of the tetrahedral network, again showing a more disordered structure in the vicinity of the subsurface density peak at low T. The results shown in Fig. 2 confirm the idea that the ions, whether single or multiple, prefer the relatively disordered high density subsurface to the relatively ordered low density tetrahedral network of the core. We note that $q_T(r)$ begins to increase beyond a minimum located at 1.6 nm, a location clearly in the surface layer where d_5 is quite high and ρ_v is nearly zero. We thus cut off the $q_T(r)$ at this minimum, as the increase is not indicative of increased tetrahedral order.

In Fig. 3, we plot for 200 K $\rho(r)$, $\rho_{\rm Na}(r)$ for a single Na ion, $q_T(r)$ and $d_5(r)$, confirming that for N = 360, 776, and 1100, the ion resides in a subsurface that is relatively disordered compared to the tetrahedral core. $\rho_{\rm Na}(r)$ decays rapidly for increasing r upon approaching the surface layer (where $d_5(r)$ radiply increases) and for decreasing r upon entering the region where $q_T(r)$ is high. The exception is the N = 100 nanodroplet, which does not have a tetrhedral core. At this size, however, layering propagating from the surface extends to the droplet interior, and it is at a minimum in $\rho(r)$ that we find the peak in $\rho_{\rm Na}(r)$. For the larger droplets too, the ion prefers to be in a trough, except for N = 1100, where layering is quite weak.

In Fig. 4 the convergence of the trajectories for Na^+ starting on the surface and the droplet center of mass is demonstrated.

B. Multiple Na^+ ions

In Fig. 2 (d) and Fig. 5, the radial distributions of multiple ions are compared at T = 300 K and 200 K in droplets comprised 776 and 1100 H_2O molecules, respectively. At T = 300 K the distributions are almost uniform with an incipient broad maximum appearing in the outer layers of the droplet.

Solution[46] of the Non-linear Poisson-Boltzmann (NPB) equation for a rigid spherical geometry suggests that toward the droplet interior the ion distribution will show an exponential decay

$$n(r) = n(R)\exp[(r-R)/\lambda_{PB}] \qquad (2)$$

where n is the ion number density, R is the sphere radius (here taken to be equal to R_e) and r is the distance from

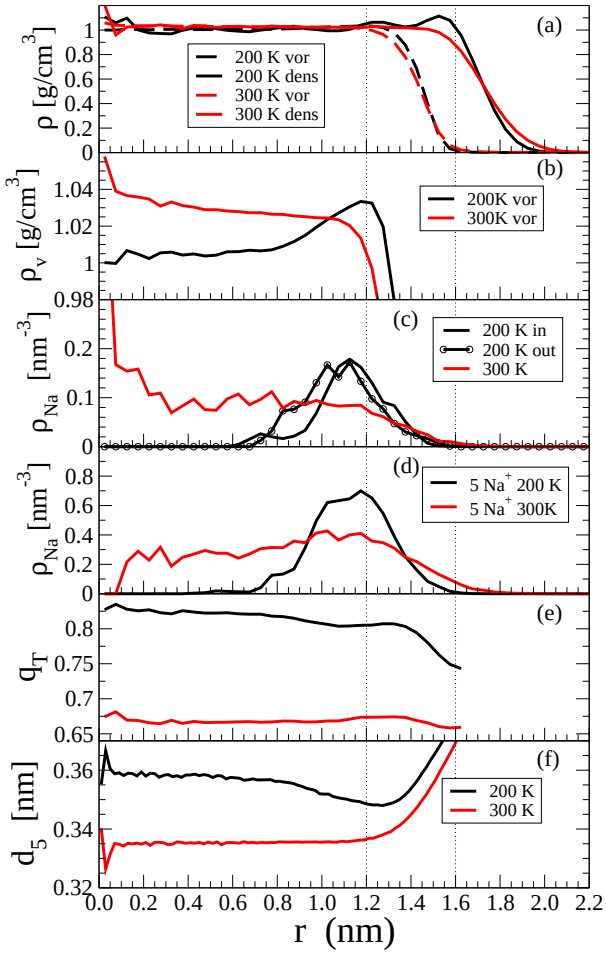

FIG. 2. Structure of pure water droplet, and single Na^+ and 5 Na^+ distributions for $N = 776$.

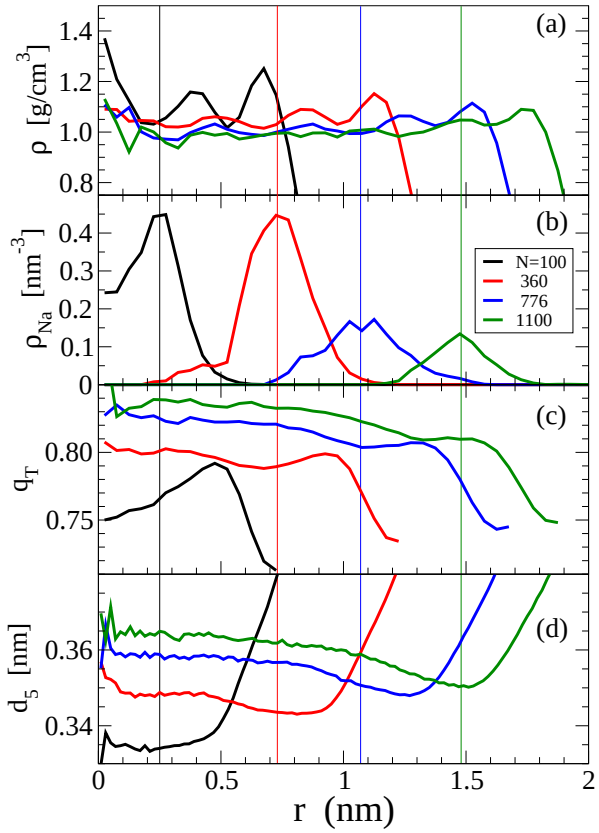

FIG. 3. Single Na^+ number density distributions and measures of structure for low temperature ($T = 200$ K) for select nanodroplet sizes $N = 100$ (black), 360 (red), 776 (blue) and 1100 (green). Shown are (a) ρ (full line) and ρ_v (dashed), (b) rho_{Na}, (c) q_T and (d) d_5, as functions or r.

the droplet center. λ_{PB} is given by

$$\lambda_{\mathrm{PB}} \approx \frac{\epsilon k_B T}{\sigma q} \tag{3}$$

where k_B is Boltzmann constant, T is temperature, ϵ is the permittivity, $q = me$ is the charge of an ion (e is the elementary positive charge) and σ is the surface charge density given by $\sigma = \frac{|Z|e}{4\pi R^2}$ ($|Z|e$ is the total droplet charge). In finding the surface charge density we assume that all the charge is in the surface. The larger the λ_{PB} the slower the ion distribution decay. The simulated ion decay cannot be exactly as the theoretical prediction because of the droplet's shape fluctuations. The larger the droplet and the lower the temperature the exponential decay will manifest more clearly. Obviously, the higher temperature will lead to a slower ion decay. For 776 H_2O molecules - 5 Na^+ ions at $T = 300$ K the distribution decays (toward the droplet's COM) as an exponential function fitted by $0.42\exp(-(1.14 - x)/1.2)$, where $\lambda_{PB} \approx 1.2$ nm. For 1100 H_2O the fitting function is $0.40\exp(-(1.37 - x)/1.3)$, where $\lambda_{PB} \approx 1.3$ nm.

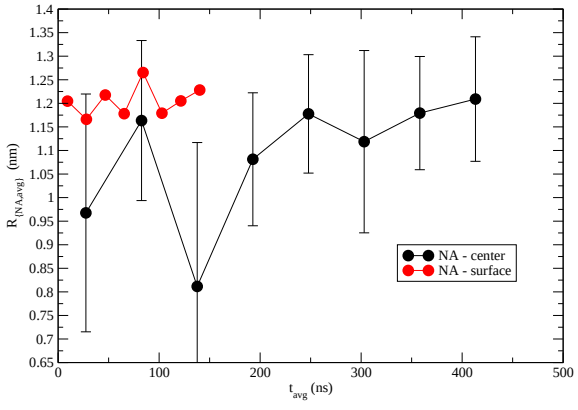

FIG. 4. Average location of ion as a function of time in a system of a single Na^+ ion and $N = 776$ at $T = 200$ K.

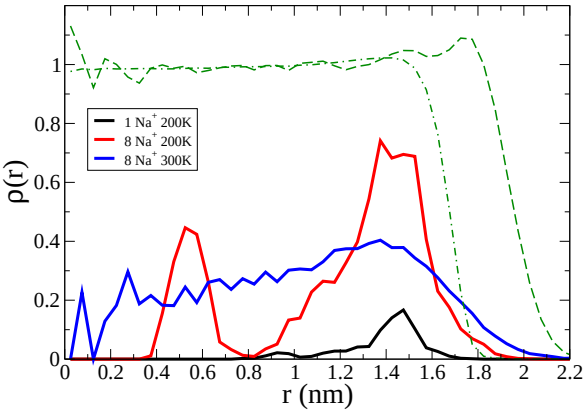

FIG. 5. Single and 8 Na^+, $N = 1100$. We are still running the 200 K data for 8 Na^+. Data are for the last 35% of the time series for 200 K.

Equation 3 with dielectric constant of water equal to 75, yields $\lambda_{PB} \approx 0.8$. In droplets of up to a few thousands of water molecules the effect of shape fluctuations is significant, therefore, we interpret the value of λ_{PB} only in a qualitative manner. The value of λ_{PB} is comparable in size with the droplet radius, which indicates that the radial distribution function will show a very slow decay toward the COM, which is in qualitative agreement with the simulations. The ion distributions at $T = 200$ K shows a decay that cannot be analyzed using the NPB. The multiple ions are expelled from the drop's core and they show a maximum at the same location as the single ion. In droplets comprised 1100 H_2O molecules - 8 Na^+ ions two peaks are observed at distance 0.52 nm and at 1.5 nm. The lower intensity peak at 0.52 nm corresponds to one ion, which can exchange with the ions that give rise to the outer peak (at $\approx$ 1.5 nm). Therefore, the appearence of two peaks does not indicate a metastable state.

Here, we can examine consequences of the ion distributions under supercooling in the charging mechanisms of macroions in native mass spectrometry (MS). In spray-based ionization methods, droplets carry the analytes from the bulk solution to the mass spectrometer. The droplets are composed of solvent, a macroion (e.g. protein, nucleic acid) and simpler ions, such as hydronium ion, Na^+, $NH_4{}^+$ ions. During their lifetime, the droplets decrease in size by solvent evaporation and ion ejection. The first question that arises is whether these droplets can be supercooled in MS experiments. The temperature of the droplets in ESI experiments is still an open question despite the insightful experiments that have been performed[47, 48]. The lack of consensus on a droplet's temperature during its lifetime is due to dependence on the specific details of the experiment. Evaporative cooling is one of the factors that determines the temperature of a drop. If evaporative cooling dominates over heating due to conductive thermal transfer to a droplet from a hotter sheath gas or friction due to motion, then a droplet may become cold enough to create an internal low-density core that expels the ions to the subsurface. In larger droplets the formation of this internal structure is more facile. In microdroplets the core may be ice because the microscopic droplets are expected to follow macroscopic theories.

The second question to address is the consequence of the ion location in the droplet's disintegration mechanism. In our view the droplet structure is one of the important factors that determines the manner in which it disintegrates. Even though in this study we do not examine droplet disintegration, in previous research we have shown that the droplet structure plays a significant role in the disintegration mechanisms. In native mass spectrometry the disintegration mechanism has been hotly debated over several decades and the question is still open because of lack of direct evidence of the mechanisms. The consensus is that there are two competing mechanisms for ion ejection from droplets. The one of them, is the Rayleigh fission[49], which involves emission of a significant amount of ions when a droplet is found very close to the Rayleigh limit. The Rayleigh limit is defined as the point where the electostatic forces balance the surface forces. Decrease of the volume or increase of the charge relative to their values at the Rayleigh limit will lead to a spontaneous division of the droplet. The other is the ion evaporation mechanism[50], which may occur before the Rayleigh limit and involves the release of a single solvated ion. We think that both mechanisms are plausible, but the faster one is the dominant one. The dominant mechanism will be determined by the conditions such as temperature and partial pressure. In previous research we have argued that in minute nanodroplets (similar in size to the ones studied here) one cannot distinguish a Rayleigh fission[49, 51–53] from IEM[50, 54]. We have also argued that the IEM models that have developed by Iribarne-Thomson[50] and Labowsky et al.[54] cannot hold for minute nanodroplets. The conditions for the IEM models to hold include a low solvent evaporation rate, which provides the time for the ions to be released before the Rayleigh limit, all the ions to be found on the surface and to be electostatically screened by the solvent. Previous atomistic modeling of aqueous droplets with diameter < 16 nm at $T = 350$ K has shown that only 55%-24% of the ions from the smaller ($\approx$ 880 H_2O molecules) to the larger droplet ($\approx 6 \times 10^4$ H_2O molecules) reside in the outer droplet layers that include the ion distribution beyond its maximum. This part of the distribution is affected the most by surface fluctuations and thus, it is more susceptible to ion evaporation[30]. The number of ions in this outer layer decreases with the increase in drop size. In droplets of a few hundreds of H_2O molecules near the Rayleigh limit, the multiple ions are not electrostatically screened by the solvent because the solution is supersaturated in ions.

In light of the structure of the supercooled charged droplets, it is expected that the higher concentration of the ions in the outer layer will increase the probability of their escape before a Rayleigh fission and will accelerate the charging of macroions on the surface relative to their bulk solution counterparts. Macroions can be kinetically confined in the outer droplet layers when their diffusion rate is slower than solvent evaporation (often this can occur at elevated temperature).

Another point to clarify here is the difference between ion distribution and solvation energy in the context of the mass spectrometry models for ion ejection[55]. In models of macroion charging in droplets, the order of single ion release from a droplet has been attributed in a qualitative manner to the dominance of the droplet's electric field over ion solvation energy[55]. The model proposes that the electric field increases as the droplet reduces in size. During the shrinking, the smaller solvation energy corresponds to an earlier ejection of the ion. The ion distributions indicate that droplets can be heterogeneous due to solvent structure, thus the solvation energy of the same ion depends on its location. A single value for the solvation energy is not a sufficient quantity to explain which ions evaporate first. The ions that are released first are the ones that are subject more to the surface fluctuations. The ion distribution at distances larger than that at the maximum of the distribution are more susceptible to ejection. Therefore, the effect that the ions have in the droplet's surface tension and consequently to the size of the shape fluctuations is the relevant parameter in an ion ejection model.

IV. CONCLUSION

We find that in supercooled aqueous droplets, a heterogeneous solvent structure leads to a different ion distribution relative to that at ambient temperature. Specifically, we demonstrated that at supercooling a tetrahedral interior network can form, that expels the ions from the core region. If we scale up this phenomenon, we expect a similar structure in larger droplets. The higher concentration of the ions in the supercooled droplet's outer layer may increase the rate of an ion-evaporation mechanism (for probabilistic reason) over a Rayleigh fission and accelerate the charging of macroions and other reactions relative to their bulk solution counterparts. Models of charging of macromolecules that for simple ion ejection consider only the balance between ion solvation energy and strength of the electric field on the droplet surface cannot capture variations in ion solvation that arise from the solvent organization at various temperatures.

We present a reference model of a single ion solvation in a droplet. The model considers the energy of a fluctuating charged dielectric droplet as the sum of the electrostatic energy and the surface energy. The model finds that the energy associated with the distance of the ion from the droplet COM is quadratic in this distance. The model can be extended further by the superposition of the electrostatic confinement with other effects such as that of the ion size.

The next step in the study of supercooled droplets with single ion, is to investigate the role of the nature of the ion in its location and in particular that of proteins. When a mixture of ions is present it is interesting to find out how supercooling affects their distribution.

ACKNOWLEDGMENTS

S.C. greatly thanks Prof. D. Frenkel, Department of Chemistry, University of Cambridge, UK, and Dr. Anatoly Malevanets, The University of Western Ontario for discussions on the stability of charged systems. We acknowledge the financial support from Natural Sciences and Engineering Research Council (Canada). Computational resources were provided by ACENET and Compute Canada.

Appendix A: Single ion within a dielectric droplet

The following discussion is extension of previous work on the energy of a continuum dielectric droplet containing a single ion[53, 56]. In the model the droplet surface fluctuations are considered. The total energy of the droplet (E) is written as the sum of surface energy ($E_{\rm surf}$) and electrostatic energy ($E_{\rm el}$)[49],

$$E = E_{\rm surf} + E_{\rm el} = \gamma A + E_{\rm el} \tag{A1}$$

where γ is the surface tension and A surface area. $E_{\rm el}$ is given by

$$E_{\rm el} = -\frac{1}{2}\int\limits_{\mathbb{R}^3/V} d\mathbf{r}(\epsilon^E - \epsilon^I)\mathbf{E}\cdot\mathbf{E}_0 \tag{A2}$$

where $\mathbb{R}^3/V$ are the points in the exterior of the droplet, ϵ^I is the electric permittivity in the interior of a droplet, ϵ^E is the electric permittivity of the medium surrounding the droplet, and

$$\mathbf{E}_0(\mathbf{r}) = -\nabla\frac{Q}{4\pi\epsilon^I r}. \tag{A3}$$

The distance of a point on the droplet surface from the ion is given by:

$$\rho(\sigma) = R + \sum_{l>0,m_l} a_{l,m_l} Y_{l,m_l}(\sigma) \tag{A4}$$

where $\sigma = (\theta,\phi)$ is the spherical angle, $\rho(\theta,\phi)$ is the distance from the centre (which is at the ion), and $Y_{lm}(\theta,\phi)$ denote the spherical harmonics functions of rank m and order l. For certain shapes of droplets, such as bottlenecked shapes or shapes like an eight we should choose the center of the shape carefully, so as we do not have for

a single (θ,ϕ) more than one values of ρ. In other words, the same line intersects the shape in several points. R is the $l=0$ term in the expansion of $\rho(\sigma)$. The details of the algebra for expressing $E_{\rm surf}$ in terms of the expansion coefficients a_{l,m_l} (see Eq. A4) is given in Ref.[[53]]. The coupling of the electrostatic energy[57] to the shape fluctuations is a tedious step and one of the ways to do that is found in Ref.[[56]].

After some algebra, the total energy is given by

$$E=\frac{(\epsilon^I-\epsilon^E)Q^2}{8\pi\epsilon^I\epsilon^E R_0}\left[1-\sum_{l>0,m_l}\frac{\epsilon^I l(l-1)-\epsilon^E(l+1)(l+2)}{\epsilon^I l+\epsilon^E(l+1)}\frac{|a_{l,m_l}|^2}{4\pi R_0^2}\right]+\gamma\left[4\pi R_0^2+\frac{1}{2}\sum_{l>0,m_l}(l-1)(l+2)|a_{l,m_l}|^2\right]. \quad \text{(A5)}$$

We will show that the $l=1$ term in Eq. A5 depends on the distance squared of the ion from the droplet COM. In the algebra that follows we will use that

$$\rho^4(\sigma)=R^4+4R^3\sum_{l>0,m_l}a_{l,m_l}Y_{l,m_l}(\sigma)+\cdots. \quad \text{(A6)}$$

In Eq. A6 we keep only the two dominant terms in the summation. The remaining of the terms are neglected because they include powers ≥ 2 of $\delta r=\sum_{l>0,m_l}a_{l,m_l}Y_{l,m_l}(\sigma)$ (δr is a small perturbation relative to R).

We find the coordinates $X_{\rm COM}, Y_{\rm COM}, Z_{\rm COM}$ of the droplet COM in terms of the expansion coefficients a_{l,m_l}. In the following expressions $d\sigma=\sin\theta d\theta d\phi$.

$$\begin{aligned}Z_{\rm COM}&=\frac{1}{V}\int Z(r,\theta,\phi)d^3r=\\&\frac{1}{V}\int_{r\leq\rho,\sigma\in S^2}r\cos\theta r^2 d\sigma dr=\\&\frac{1}{4V}\int\rho^4(\theta,\phi)\cos\theta d\sigma=\\&\frac{1}{V}R^3\int\cos\theta\sum_{l>0,m_l}a_{l,m_l}Y_{l,m_l}(\sigma)d\sigma=\\&\left(\frac{3}{4\pi}\right)^{1/2}a_{1,0}\end{aligned} \quad \text{(A7)}$$

In the fourth line of Eq. A7 we use the orthogonality of the spherical harmonics. Similarly $X_{\rm COM}=\Re(a_{1,1})\sqrt{2}$ and $Y_{\rm COM}=\Im(a_{1,1})\sqrt{2}$.

The $l=1$ term in Eq. A5 yields

$$\Delta E_1=\frac{(\epsilon^I-\epsilon^E)Q^2}{8\pi\epsilon^I\epsilon^E R_0}\frac{6\epsilon^E}{\epsilon^I+2\epsilon^E}\frac{(|a_{1,0}|^2+|a_{1,1}|^2+|a_{1,-1}|^2)}{4\pi R_0^2} \quad \text{(A8)}$$

Using Eq. A7 and the similar ones for $X_{\rm COM}$ and $Y_{\rm COM}$, Eq. A8 becomes

$$\Delta E_1(\mathbf{r})=\frac{\varepsilon-1}{4\pi\epsilon_0\varepsilon(\varepsilon+2)}\frac{Q^2}{R^3}\|\mathbf{r}\|^2 \quad \text{(A9)}$$

where Q, R and ε are the charge of the ion, the droplet radius and the relative dielectric constant of the solvent, respectively, ε_0 is the vacuum permittivity and $\|\mathbf{r}\|^2=X_{\rm COM}^2+Y_{\rm COM}^2+Z_{\rm COM}^2$. The energy (A9) has the functional form of a harmonic potential. From this point we would refer to this effect as "electrostatic confinement" (EC) for the lack of a better term. We introduce the spring constant $K(\varepsilon)$ where

$$K(\varepsilon)=\frac{\varepsilon-1}{4\pi\epsilon_0\varepsilon(\varepsilon+2)}\frac{Q^2}{R^3}. \quad \text{(A10)}$$

In Fig. 6 we plot the value of the spring constant as a function of the relative dielectric constant for a droplet comprising 1000 water molecules and an ion. The electrostatic energy has two limiting cases $\varepsilon=1$ and $\varepsilon=\infty$ when the electrostatic interaction of the ion with the droplet surface vanishes. In the former case the external and internal dielectric constants are equal and the droplet does not perturb the electric field of the ion. In the latter case the electrostatic field in localized in the vicinity of the ion and it is not affected by the droplet surface. As seen in the plot the maximum of the coefficient $K(\varepsilon)$ is attained at $\varepsilon=1+\sqrt{3}\approx 2.73$.

If the ion is localized in the center of a droplet the Gibbs-Boltzmann distribution of the ion positions is given by

$$P(\|\mathbf{r}\|^2)=\frac{2}{\sqrt{\pi}}\left(\frac{K(\varepsilon)}{k_BT}\right)^{3/2}\|\mathbf{r}\|e^{-K(\varepsilon)\|\mathbf{r}\|^2/k_BT}. \quad \text{(A11)}$$

The expectation value of the square of the distance of the ion from the center of mass is given by

$$\langle\|\mathbf{r}\|^2\rangle=\frac{3}{2}\frac{k_BT}{K(\varepsilon)} \quad \text{(A12)}$$

The EC is more pronounced when the ion is localized at the center of the droplet, therefore we can write $\langle\|\mathbf{r}\|^2\rangle/R^2\ll 1$. Analysing Eqs. (A10) and (A12) we conclude that the effect will be more pronounced at low temperature, high charge, small radius and intermediate values of the dielectric constant. Small droplet with high charge may undergo Rayleigh instability[58]. If this is an issue in observations we need to increase the droplet radius while keeping constant the value of the Rayleigh parameter $X\sim Q^2/R^3$. To illustrate the EC we model high charges by creating models of charged cyclic peptides. DNA and RNA strands are other examples where the effect of the EC will be clearly observed.

	Size [N]	Charge [Z]	K [mJ/m^2]	$\langle\|\|\mathbf{r}\|\|^2\rangle$ [nm^2]
Theor. ϵ =80	1000	1 e$^+$	0.40	15.3
Sim. Gamma	1000	1 e$^+$	4.53	1.36
Sim. Confinement	1000	1 e$^+$	< 0.83	1.36
Sim. Gamma	1000	3 e$^+$	20.7	0.30
Theor. ϵ =38	1000	3 e$^+$	20.5	0.30

TABLE II. Values of the parameter K for selected simulations of an ion in a droplet.

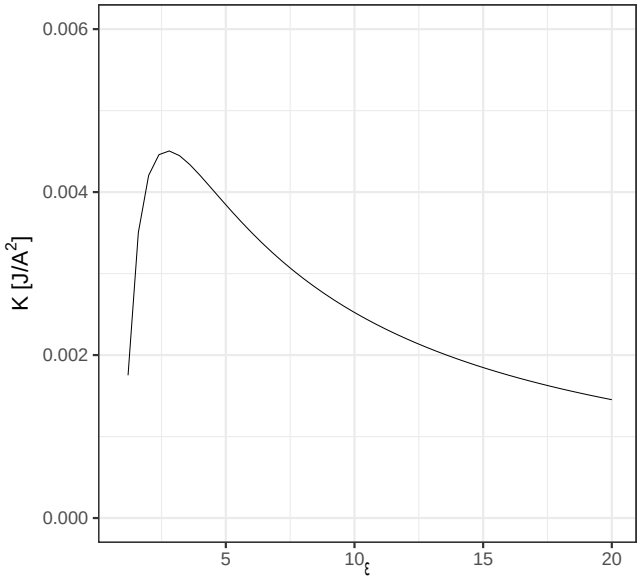

FIG. 6. Magnitude of the spring constant as a function of the relative dielectric constant ε is plotted. The values correspond to an ion of charge $Q = 1e$ in a droplet comprising 1000 water molecules and the radius 19Å. The value of the potential has a maximum at $\varepsilon \approx 1 + \sqrt{3} \approx 2.73$.

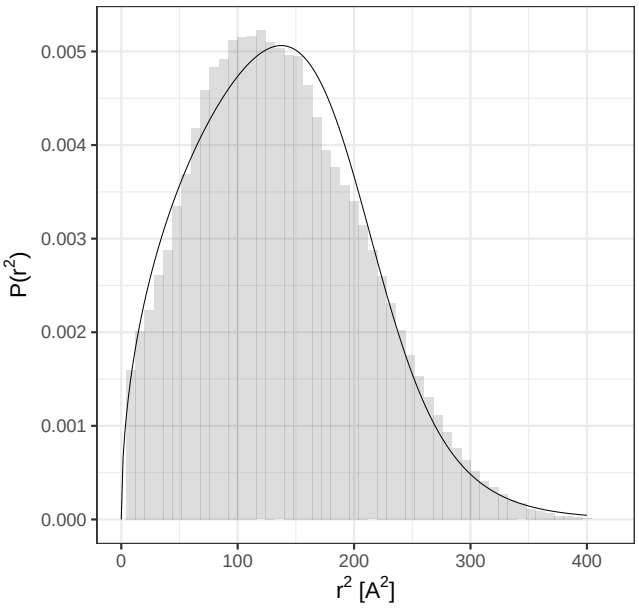

FIG. 7. The distribution of the distances of the sodium ion relative to the COM of the droplet is plotted. The equimolecular droplet radius is 1.9 nm. The solid line is the product of the logistic and the gamma functions intended to capture confinement effects. The function is fitted to the distribution using MLE.

Using the maximum value of the K parameter from Fig. 6 we obtain the estimate of the minimal dimensions of the excursions of the ion from its equilibrium position at the center of the droplet $\sqrt{\langle\|\mathbf{r}\|^2\rangle} \geqslant 12$Å. Therefore, for a droplet comprising 1000 water molecules and a single charge $Q = 1e$ the confining effects should be taken into consideration.

We assume that the number density of the solvent in the vicinity of the droplet surface is well approximated by the logistic function (A13)

$$n_{r_0,d}(r) = \frac{1}{1 + \exp(-(r - r_0)/d)} \tag{A13}$$

where d and r_0 are fitting parameters that can be interpreted as the droplet radius and the width of the surface layer. Using the logistic curve for for the number density (entropic factor) and gamma function that takes into account the electric potential (energetic factor) we arrive at the following ansatz for the ion distribution

$$p(r^2) \sim re^{-Kr^2/k_BT} \frac{1}{1 + \exp(-(r - r_0)/d)} \tag{A14}$$

Using the maximum likelihood approach we found the most probable parameters $\{K, r_0, d\}$ in order to match the observed values of the distance of the ion from the center of mass. In Fig. 7 we show the fitted and the observed distributions for a single sodium ion in a droplet of 1000 TIP3p water molecules. The data were obtained in XXXns molecular dynamics simulations using the NAMD package[59]. The fits were produced with the use of statistical analysis software R[60]. For comparison we contrast the fit that takes into account the surface of the droplet with a fit to a gamma function of shape 1/2 in Fig. 8. The analysis shows that the shape fluctuations of the droplet accounts for the distribution of the ions in the droplet. The fitting can only establish an upper bound of the parameter K. All the variability of the

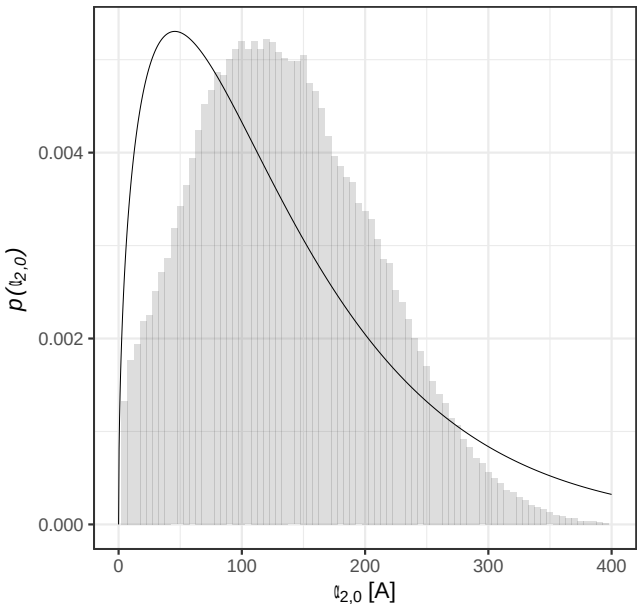

FIG. 8. Same as Fig. 7 but the solid line is the gamma function fitted to the distribution using MLE.

charge distribution is explained by the confinement effect of the droplet surface. In Fig. 7 the fitting parameters used in Eq. (A14) are $r_0 = 14.9$Å and $d = 1.1$Å. The effective radius of the droplet is smaller than that of the true molecular surface of water.

The results of the simulations of a sodium ion in water droplet can be compared with the results of the simulations of a cyclic peptide. In Fig. 9 the distribution of the distance of the center of mass of the peptide relative to the COM of the droplet is plotted. The droplet radius is 1.9 nm and the charge is $3e^+$. The distribution tapers off before reaching the droplet surface. Sampling proves to be a challenge in such systems. The simulation time should be much longer than the time for a molecule to diffuse the width of the droplet $Dt_{\rm sim} \gg R^2$. Typical values of the diffusion coefficient (D) are $\sim 10^{-9}[\frac{\rm m^2}{\rm s}]$, hence the simulation time has to be in 10 ns 100 ns range at temperature $T = 300$K.

The estimated values of the dielectric constant are lower that the typical values of the pure solvent. We believe that the apparent decrease in the dielectric constant is connected with the saturation of the polarization in the vicinity of the charge ion.

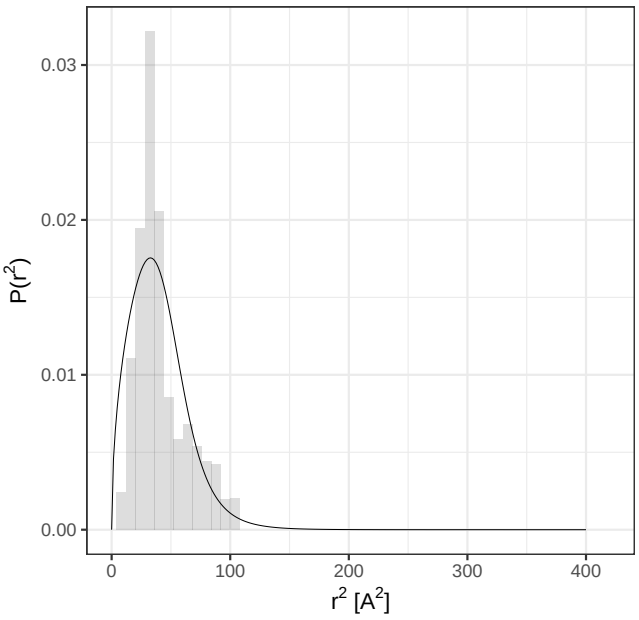

FIG. 9. The distribution of the distances of the center of mass of the peptide relative to the COM of the droplet is plotted. The droplet radius is 3.8 nm and the charge is $8e^+$. The solid line is the gamma function fitted to the distribution using MLE.

[1] R. M. Bain, C. J. Pulliam, and R. G. Cooks, Chem. Sci. **6**, 397 (2015).
[2] A. J. Ingram, C. L. Boeser, and R. N. Zare, Chem. Sci. **7**, 39 (2016).
[3] T. Sahraeian, D. S. Kulyk, and A. K. Badu-Tawiah, Langmuir **35**, 14451 (2019).
[4] D. Lu and S. J. Singer, The Journal of chemical physics **105**, 3700 (1996).
[5] O. Gorlova, J. W. DePalma, C. T. Wolke, A. Brathwaite, T. T. Odbadrakh, K. D. Jordan, A. B. McCoy, and M. A. Johnson, J. Chem. Phys. **145**, 134304 (2016).
[6] D. H. Herce, L. Perera, T. A. Darden, and C. Sagui, The Journal of chemical physics **122**, 024513 (2005).
[7] L. Perera and M. L. Berkowitz, Zeitschrift für Physik D Atoms, Molecules and Clusters **26**, 166 (1993).
[8] F. Thaunay, G. Ohanessian, and C. Clavaguera, Chemical Physics Letters **671**, 131 (2017).
[9] Y. Zhao, H. Li, and X. C. Zeng, Journal of the American Chemical Society **135**, 15549 (2013).
[10] D. Hagberg, S. Brdarski, and G. Karlström, The Journal of Physical Chemistry B **109**, 4111 (2005).
[11] C. J. Burnham, M. K. Petersen, T. J. Day, S. S. Iyengar, and G. A. Voth, The Journal of chemical physics **124**, 024327 (2006).
[12] G. Makov and A. Nitzan, The Journal of Physical Chemistry **98**, 3459 (1994).
[13] J. J. Fifen and N. Agmon, Journal of chemical theory and computation **12**, 1656 (2016).
[14] M. Galib, M. Baer, L. Skinner, C. Mundy, T. Huthwelker, G. Schenter, C. Benmore, N. Govind, and J. L. Fulton, The Journal of chemical physics **146**, 084504 (2017).
[15] L. Perera and M. L. Berkowitz, The Journal of chemical

physics **96**, 8288 (1992).
[16] L. Perera and M. L. Berkowitz, The Journal of Chemical Physics **99**, 4236 (1993).
[17] L. Perera and M. L. Berkowitz, The Journal of chemical physics **95**, 1954 (1991).
[18] C. Caleman, J. S. Hub, P. J. van Maaren, and D. van der Spoel, Proceedings of the National Academy of Sciences **108**, 6838 (2011).
[19] J. C. Werhahn, D. Akase, and S. S. Xantheas, The Journal of chemical physics **141**, 064118 (2014).
[20] S. Vaitheeswaran and D. Thirumalai, Journal of the American Chemical Society **128**, 13490 (2006).
[21] E. Harder and B. Roux, The Journal of chemical physics **129**, 12B613 (2008).
[22] P. Wang, R. Shi, Y. Su, L. Tang, X. Huang, and J. Zhao, Frontiers in chemistry **7**, 624 (2019).
[23] F. Fracchia, G. Del Frate, G. Mancini, W. Rocchia, and V. Barone, Journal of chemical theory and computation **14**, 255 (2018).
[24] D. J. Miller and J. M. Lisy, J. Am. Chem. Soc. **130**, 15381 (2008).
[25] M. W. Ross, C. Berkdemir, and A. Castleman Jr, J. Phys. Chem. A **116**, 8530 (2012).
[26] S. Chakrabarty and E. R. Williams, Phys. Chem. Chem. Phys. **18**, 25483 (2016).
[27] O. M. Cabarcos, C. J. Weinheimer, T. J. Martınez, and J. M. Lisy, The Journal of chemical physics **110**, 9516 (1999).
[28] Y. Marcus, Chemical reviews **109**, 1346 (2009).
[29] V. Kwan, A. Malevanets, and S. Consta, The Journal of Physical Chemistry A **123**, 9298 (2019).
[30] V. Kwan and S. Consta, Chemical Physics Letters , 137238 (2020).
[31] V. Kwan and S. Consta, Journal of the American Society for Mass Spectrometry **0**, null (2020), pMID: 32597645.
[32] S. M. A. Malek, P. H. Poole, and I. Saika-Voivod, Nat. Commun. **9**, 2402 (2018).
[33] J. C. Johnston and V. Molinero, Journal of the American Chemical Society **134**, 6650 (2012).
[34] P. K. Nandi, C. J. Burnham, Z. Futera, and N. J. English, ACS Earth and Space Chemistry **1**, 187 (2017).
[35] T. Li, D. Donadio, and G. Galli, Nature communications **4**, 1 (2013).
[36] A. Haji-Akbari and P. G. Debenedetti, Proceedings of the National Academy of Sciences **114**, 3316 (2017).
[37] v. d. S. D. Berendsen, H. J. C. and R. van Druren, Comput. Phys. Commun. **91**, 43 (1995).
[38] H. B. Lindahl, E. and D. van der Spoel, J. Mol. Model. **7**, 306 (2001).
[39] L. E. H. B. G. M. A. E. van der Spoel, D. and H. J. C. Berendsen, J. Comput. Chem. **26**, 1701 (2005).
[40] K. C. v. d. S. D. Hess, B. and E. Lindahl, J. Chem. Theory Comput. **4**, 435 (2008).
[41] J. L. F. Abascal and C. Vega, J. Phys. Chem **123**, 234505 (2005).
[42] J. Aqvist, The Journal of Physical Chemistry **94**, 8021 (1990).
[43] P. L. Chau and A. J. Hardwick, Mol. Phys. **93**, 511 (1998).
[44] S. M. A. Malek, P. H. Poole, and I. Saika-Voivod, J. Chem. Phys. **150**, 234507 (2019).
[45] J. L. Aragones, L. G. MacDowell, and C. Vega, J. Phys. Chem. A **115**, 5745–5758 (2010).
[46] A. Malevanets and S. Consta, The Journal of chemical physics **138**, 184312 (2013).
[47] A. Soleilhac, X. Dagany, P. Dugourd, M. Girod, and R. Antoine, Analytical chemistry **87**, 8210 (2015).
[48] S. C. Gibson, C. S. Feigerle, and K. D. Cook, Analytical chemistry **86**, 464 (2013).
[49] L. Rayleigh, Philos. Mag. **14**, 184 (1882).
[50] J. V. Iribarne and B. A. Thomson, J. Chem. Phys. **64**, 2287 (1976).
[51] J. Peters, Eur. J. Phys. **1**, 143 (1980).
[52] C. Hendricks and J. Schneider, Am. J. Phys **31**, 450 (1963).
[53] S. Consta and A. Malevanets, Mol. Simul. **41**, 73 (2015).
[54] M. Labowsky, J. Fenn, and J. F. de la Mora, Analytica Chimica Acta **406**, 105 (2000).
[55] C. J. Hogan Jr, J. A. Carroll, H. W. Rohrs, P. Biswas, and M. L. Gross, Anal. Chem. **81**, 369 (2009).
[56] M. I. Oh, A. Malevanets, M. Paliy, D. Frenkel, and S. Consta, Soft Matter **13**, 8781 (2017).
[57] J. D. Jackson, *Classical Electrodynamics*, third ed. ed. (John Wiley & Sons, New York, NY, 1998).
[58] S. Consta, J. Phys. Chem. B **114**, 5263 (2010).
[59] J. C. Phillips, R. Braun, W. Wang, J. Gumbart, E. Tajkhorshid, E. Villa, C. Chipot, R. D. Skeel, L. Kalé, and K. Schulten, J. Comput. Chem. **26**, 1781 (2005).
[60] R Core Team, *R: A Language and Environment for Statistical Computing*, R Foundation for Statistical Computing, Vienna, Austria (2017).